Topological Hydrogen-Bond Saturation as a Design Route to Type V Deep Eutectics.

Alessandro Triolo[1,*], Emanuela Mangiacapre[2], Vitaly V. Chaban[3], Fabrizio Lo Celso[4], Franca Castiglione[5], Laszlo Almasy[6], Barbara Fazio[7], Olga Russina[2,*]

[1] Laboratorio Liquidi Ionici, Istituto Struttura della Materia, Consiglio Nazionale delle Ricerche (ISM-CNR), Rome 00133, Italy

[2] Department of Chemistry, University of Rome Sapienza, Rome 00185, Italy

[3] XXXX

[4] Department of Physics and Chemistry, Università di Palermo, Palermo, Italy

[5] Department of Chemistry, Materials and Chemical Engineering "Giulio Natta", Politecnico di Milano, 20133 Milan, Italy

[6] XXXX

[7] XXXX

[*] Corresponding authors: A. Triolo (alessandro.triolo@cnr.it); O. Russina (olga.russina@uniroma1.it)

Abstract

Type V deep eutectic solvents, formed by combination of neutral hydrogen-bonding molecules, remain difficult to predict and engineer. The recent proposal that the asymmetric nature of hydrogen bonding (HB) donor and acceptor capability of precursors might be a key approach for their formulation requires validation. Here we show that the emergence of a topologically saturated hydrogen-bond network provides a mechanistic route to formulate such systems, exemplified by the carvacrol–dimethyl sulfoxide (DMSO) mixture. COSMO-RS screening predicts a profoundly deep eutectic (about 110 K depression) arising from donor-free, strong HB acceptor DMSO when paired with asymmetric HB donor carvacrol.

To our knowledge, this is the first example of a type V DES whose precursors are liquid at ambient conditions, thus enabling a detailed exploration of chemical physical properties and their excess values to be probed across the whole composition window.

This approach is fundamental to describe the complex structural and dynamical organisation of carvacrol–DMSO mixtures across composition and relate hydrogen-bond topology to the onset of deep eutectic behaviour, on the basis of complementary thermophysical measurements, neutron scattering, NMR and classical molecular dynamics simulations.

The work addresses two main points: a) can present knowledge be used to custom engineer type V DES? and b) how the do evolution and competition of intra- and inter-species interactions, across the whole composition range, lead to the large depth in the eutectic behaviour of type V DES?

Introduction.

Deep eutectic solvents (DESs) embody the principle that mixtures can be engineered to melt far below their components, by favouring unlike over like–like interactions. Since their first discovery in 2003 by Abbott[1,2], who demonstrated that choline chloride forms low-melting mixtures when combined with urea, a wide range of related compounds has been proposed, classifying them in multiple classes, on the basis of the nature of their precursors. More recently, Coutinho and collaborators introduced the concept of a fifth class (type V)[3–5], which is composed entirely of neutral molecules, yet retaining the thermodynamic hallmark of "deep" behaviour: large negative deviations from the ideal liquidus line.

What makes a eutectic mixture "deep" is its ability to display a melting-point depression far greater than expected for an ideal mixture. In thermodynamic terms, this corresponds to strong negative deviations from the ideal liquidus line, arising when the interactions between unlike species are substantially stronger than those within the pure components. Type V DESs are particularly intriguing because they achieve deep character in the absence of ionic species, thereby suppressing dominant Coulombic interactions that would otherwise mask how directional H-bonding, dispersion, and packing anisotropy might govern eutectic depth.

Hydrogen bonding has consistently been identified as a central driving force behind the unusual stability and properties of DESs.[6–8] Yet, the establishment of hydrogen-bonding interactions across the bulk liquid does not automatically ensure the emergence of deep eutecticity[9]. Focusing on type V DESs, Coutinho and co-workers underscored the importance of combining asymmetric hydrogen-bond donors (HBD), which behave as strong donors but poor acceptors, with strong HB acceptors (HBA) that lack donor capability.[3,4,10] This asymmetry in hydrogen-bonding capability allows for preferential donor–acceptor interactions that stabilize the mixture more effectively than those present in the pure components.

In this context, the most well-known example of an asymmetric HBD is thymol. This terpene molecule possesses a hydroxyl group that is more positive than in a typical alcohol. This unusual behavior arises from resonance effects that delocalize the oxygen's lone pairs across the aromatic ring, making the hydroxyl group more positively polarized than in a typical alcohol. As a consequence, thymol functions as a weak HBA, but an unusually strong HBD. In its pure liquid, this imbalance produces hydrogen bonds between a good donor and a poor acceptor, while in mixtures with suitable partners the strong donor capacity of thymol can give rise to particularly stabilizing interactions, reflected in pronounced negative deviations from ideality.

Building on this rationale, Coutinho and co-workers also pointed out that efficient hydrogen-bond acceptors for type V DESs are those that lack donor sites. Examples include ketones, aldehydes, and tertiary amines, which cannot self-associate but form stabilizing interactions when paired with asymmetric donors.

Representative candidates proposed in the literature include 1,5-diazabicyclo[5.4.0]undec-5-ene (DBU)[11], trioctylphosphine oxide (TOPO)[12], and cyclodextrins[13–16].

Carvacrol[17,18] is a regioisomer of thymol. Like thymol, it exhibits asymmetric HBD behavior, acting as a strong donor but a weak acceptor. Unlike thymol, however, carvacrol is liquid at room temperature, with a melting point of 274.2 K. Its lower melting enthalpy ($\Delta Hm = 11.49$ kJ mol^{-1}) and entropy ($\Delta Sm = 41.89$ J mol^{-1} K^{-1}) make it particularly prone to forming eutectic mixtures with depressed melting points. For example, Alhadid and co-workers showed that, although the menthol/thymol system exhibits larger deviations from the ideal liquidus line, the menthol/carvacrol system reaches an even lower eutectic temperature, around 243.35 K at carvacrol molar fraction, Xc, equal to 0.58.[19]

Dimethyl sulfoxide (DMSO) is a strong hydrogen-bond acceptor (HBA) and lacks any donor site: its polarized S=O group avidly captures phenolic H donors, promoting hetero-association and stabilizing a connected H-bond network. It then nicely fits into the proposed class of compounds that might successfully deliver a deep eutecticity, when paired with a suitable asymmetric HBD.

Accordingly, the carvacrol–DMSO binary system represents a minimal, well-controlled testbed for the above described proposal by Coutinho and co-workers: it lets us probe the microscopic origins of deep eutecticity in type V media, without ions or competing HB motifs that might blur interpretation. Equally important, both components are liquids at ambient conditions, so the system remains fluid across the entire composition range, enabling a seamless, composition-resolved exploration of thermos-physical and structural properties.
From the perspective of safety and environmental impact, the selected species also offer a potentially appealing profile. Carvacrol, being plant-derived, is generally recognized as safe (GRAS) and additionally exhibits antimicrobial and antioxidant activities, though its strong bioactivity requires careful control of conditions of use. DMSO is of low intrinsic toxicity but demands caution due to its ability to facilitate dermal absorption of other chemicals.

In this contribution, we therefore aim at filling the following key knowledge gaps: i) *can we engineer a mixture to deliver deep eutectic behaviour, on the basis of the existing theories?* and ii) *what is the role of competing interactions in shaping the DES behaviour?*

Despite the central role of hydrogen bonding in DESs, deep eutecticity does not stem from local H-bonds alone; it emerges when asymmetric HB functionality biases network topology with composition, suppressing like–like self-association and favoring directional cross links. Crucially, this asymmetry makes a composition

threshold likely: as HB stoichiometry approaches saturation, the network reorganizes - transitioning from isolated HB interacting clusters to a medium-range framework - so that specific interactions, packing efficiency, and mesoscopic structure co-evolve to yield characteristic chemical physical properties.

Our working hypothesis is a connectivity-driven crossover: as composition evolves, the O–H···O=S network in carvacrol-DMSO mixtures approaches topological saturation, imposing cooperative constraints that compact the liquid and hinder molecular mobility, thereby stabilizing the liquid relative to the solid (i.e., deepening the eutectic).

To test this picture, we integrate thermo-physical measurements (density, viscosity, self-diffusion) and their excess functions with atomistic molecular dynamics (MD) and scattering at complementary length scales, to deliver a coherent, composition-resolved account of the thermodynamic, structural, and dynamical signatures that mark the onset of deep eutectic behavior.

By centering the study on a single, mechanistically transparent pair—an asymmetric donor (carvacrol) with an over-achieving acceptor (DMSO)—this manuscript aims to clarify when and how type V mixtures become "deep." Beyond establishing the structure vs. property map for carvacrol–DMSO, the results articulate design rules for neutral DESs: tune composition to the connectivity window where donor–acceptor bonding is both strong and spatially organized, and expect co-ordinated signatures across excess properties, structural features and transport. This provides a practical blueprint for formulating type V media with targeted fluidity, solvating power, and thermal behavior. For example by positioning formulation inside or outside the connectivity window, one can dial fluidity, diffusivity, and solvation power for tasks such as selective dissolution (e.g., lignin/cellulose fractions), viscosity matching for processing and printing, rate control in catalysis and electrochemistry, and stability of reactive intermediates. The proposed approach also enables predictive screening - combining COSMO-RS with MD - to target donor/acceptor pairs and compositions that maximize deep-eutectic benefits while avoiding regimes where transport becomes too sluggish for the intended application.

Materials & Methods

Experimental.

Carvacrol (carv) was a TCI product (99.6%) while dimethyl sulfoxide (DMSO) a Sigma Aldrich compound (99.9 %). Compounds were mixed into a glove-box to ensure a dried environment. Mixtures with a different amount of carvacrol in terms of carvacrol molar fraction, Xc, ranging from 0.1 to 0.9 were prepared. The mixtures were then kept at room temperature (298 K) under constant agitation to obtain transparent and homogenous liquids. Mixtures prepared in such a way were sealed and maintained at ambient conditions until ready for further characterizations.

Density (ρ) measurements were carried out using a Mettler Toledo DM45 DeltaRange density meter. Prior to analysis, the instrument was calibrated with dry air and bi-distilled water at 293 K. Measurements were conducted over the temperature range 278–333 K. For mixtures with Xc = 0.1 and 0.2, the temperature range was limited to 293–333 K, while for pure DMSO measurements were performed between 298 and 333 K. Experimental density values were used to extract excess molar volume values, following the formula:

$$\Delta V_m = \left(\frac{x_1 \cdot MW_1 + x_2 \cdot MW_2}{\rho}\right) - \left(\frac{x_1 \cdot MW_1}{\rho_1} + \frac{x_2 \cdot MW_2}{\rho_2}\right),$$

where x_i and MW_i are mole fraction and molar mass of the i-th component, and ρ, ρ_1 and ρ_2 are the densities of the mixture and of the pure components at the same temperature, respectively.

Excess molar volume features deliver information on the competition between specific interactions (e.g. HB, dipole–dipole interactions) and steric/free-volume and packing efficiency or structural evolution (e.g. clustering) when mixing the precursors. Negative values for ΔV_m fingerprint the establishment of strong hetero-interactions and efficient fit (e.g., O–H···O=S complexation, shape/size complementarity) that draw components closer than like–like contacts would; on the other hand, positive values are the consequences of packing frustration or weak/repulsive cross-interactions (size/shape mismatch, disrupted local order, incomplete coordination).

Dynamic viscosity (η) measurements were performed using an Anton Paar micro-viscometer (Lovis 2000 M/ME) with an accuracy of up to 0.5%. Temperature control was achieved via Peltier elements (precision ±0.02 K). Measurements were carried out between 278 and 333 K; for mixtures with Xc =0.1 and 0.2 the temperature range was restricted to 293–333 K, while for pure DMSO, measurements were performed between 298 and 333 K. Depending on the viscosity range, calibrated glass capillaries with internal diameters of 1.59 mm or 1.80 mm were employed. Viscosity data were modelled using the Vogel-Fulcher-Tammann formula: $\eta = \eta_0 \cdot e^{\frac{D}{T - T_{VF}}}$; where η, D and T_{VF} are empirical parameters, accounting for deviations from ideal Arrhenius-like behaviour.

Experimental viscosity values were used to extract excess viscosity values, following the formula:

$$\Delta\eta = \eta - (x_1 \cdot \eta_1 + x_2 \cdot \eta_2),$$

where η and η_i are viscosities of the mixture and the neat i-th component, and x_i are the molar fractions of the i-th component in the mixture, respectively. Negative values fingerprint disruption of like–like cages/self-association, lubrication by a smaller or weakly interacting component, and lower activation barriers for flow. Positive values, instead, hint for strong hetero-association (e.g. stronger HB interactions or longer HB lifetimes), transient network/cluster formation, and enhanced caging/orientational order that hinder rearrangements.

NMR measurements were performed on all the carvacrol-DMSO mixtures using a Bruker Avance NEO 400 MHz spectrometer (9.4 T). Approximately 0.7 mL of each mixture was transferred into a 5 mm NMR tube. A sealed capillary containing deuterated water (D_2O) was inserted in each tube and used as an external lock and chemical-shift reference. ^{1}H NMR spectra were acquired at room temperature (298 K), and the spectra were processed using MestReNova 15.0.0-34764. Diffusion-ordered spectroscopy (DOSY) experiments were performed using the bipolar pulse-pair longitudinal eddy-current delay (BPP-LED) pulse sequence. The experimental parameters were: gradient pulse duration δ = 1.5–3 ms, diffusion delay Δ = 0.1–0.5 s, 8 scans, and a relaxation delay of 10 s. The pulsed-field gradients were linearly increased from 2% to 95% of the maximum amplitude in 32 steps. A gradient system capable of generating sine-shaped magnetic-field pulses up to 53 G cm^{-1} along the z-axis was employed. All DOSY spectra were visualized using Bruker Dynamics Center version 2.8.6. All measurements were performed at 298 K.

SANS

Computational details.

Molecular dynamics simulations were performed using the GROMACS 2021.3 package.[20,21] Bonded and non bonded parameters for dimethyl sulfoxide (DMSO) and carvacrol were described using an all-atoms potential OPLS-AA force field.[22] OPLS-AA non bonded parameters for carvacrol were changed with respect to our previous reports on this compound [23,24], to reproduce experimental density and diffusion coefficient; further details are described in the next section. The simulations were performed using a cubic box containing 1200 and 4000 molecules for the pure systems, carvacrol and DMSO, respectively. Regularly spaced in molar concentration mixtures were simulated in the carvacrol molar fraction, Xc, regime between 0.1 and 0.9, every 0.1 (for a total of 9 mixtures), the total number of atoms was chosen to keep the final box side length at least 90 Å; periodic boundary conditions were applied. Force field parameter files were created by LipParGen webserver for carvacrol and thereby modified;[25] DMSO parameters were directly downloaded from the OPLSA section of the server https://virtualchemistry.org/ff.php. Initial configurations were created by

Packmol software.[26] The starting density for each composition and each of the pure solvents was fixed about 10% lower than the experimental ones. The equilibration procedure was done in several steps, starting from a 2 ns NVT simulation at 400 K, followed by a series of 2 ns NPT runs lowering progressively the temperature to 350 K and then to 300 K at 1 bar. After the equilibration phase, the system was run for a total of 20 ns for a production run (300 K and 1 bar), and then a trajectory of 4 ns was saved at a frequency of 1 ps for the calculation of the structural properties. During the production runs for the temperature coupling, we used a velocity rescaling thermostat [27] (with a time coupling constant of 1 ps), while for the pressure coupling, we used a Parrinello–Rahman barostat[28] (10 ps for the relaxation constant). The Leap-Frog algorithm with a 2.0 fs time step was used for integrating the equations of motion. Cut-offs for the Lennard-Jones and real space part of the Coulombic interactions were set to 15 Å. For the electrostatic interactions, the Particle Mesh Ewald (PME) summation method [29,30] was used, with an interpolation order of 6 and 0.08 nm of FFT grid spacing. Selected pair correlation functions, angular distribution functions and spatial distribution functions were obtained using TRAVIS [31–33]. Densities, mean square displacement and diffusion coefficients were obtained by means of Gromacs gmx energy utility.[20,21]

Force Field parametrization.

To refine the OPLS/AA force field for the carvacrol molecule, its monomer and dimer were simulated at the hybrid density functional theory (HDFT) M11/TZVP level of theory.[34] The combination of the HDFT framework with an atom-centered split-valence triple-zeta polarized basis set [35] provided an optimal balance of chemical reliability and computational cost. All involved geometries of monomers and dimers were optimized by the rational function optimization algorithm before fitting the ab initio electrostatic potential to the set of point atomic charges used in MD. The Merz-Kollman scheme was employed.[36]

Figure S1 exemplifies the optimized geometries of carvacrol in implicit dichloroethane. This solvent exhibits a dielectric constant, which is similar to those of phenols. The polarized continuum model was used to implement implicit solvation. GAMESS.2020 quantum-chemistry program was used. [37]

In a dimer of carvacrol, an intermolecular medium-strength 197 pm-long H bond emerges, uniting the hydroxyl groups of the adjacent molecules. In turn, the O H covalent bond length amounts to 97 pm as expected. The carvacrol molecules are mutually arranged to maximize the energy of H bonding and the energy of phenyl-phenyl attractions, whereas the aggregation of the non-polar moieties is suppressed in the lowest-energy dimer configuration.

Partial charges are the cornerstone of a reliable force field model for classical MD. The effect of solvents of various polarities on the electronic density distribution over the carvacrol molecule was evaluated (**Table S1 in the ESI**). Compared to vacuo, implicit solvents polarize carvacrol in most cases, with the effect of water

exceeding the effect of dichloroethane. The charges obtained in implicit dichloroethane were prioritized in the course of force field refinement.

The effect of H-bonding on the distribution of partial charges was investigated by comparing the carvacrol monomer to the carvacrol dimer (**Table S2 in the ESI**). The effect of pairing was found to be insignificant, which is probably related to a relative weakness of the occured O…H bonding. This observation suggests that the MD simulation of the condensed phase of carvacrol should be reliable even without a specific force field correction for H-bonded dimers.

The refinement of the OPLS/AA model was carried out by considering the experimental properties – such as density, dynamic viscosity, and self-diffusion coefficients – measured in the present work. First, the computed charges were assigned by averaging the numbers over symmetrically equivalent interaction sites in the optimized structure of the monomer. The overall electrostatic neutrality of carvacrol was hereby preserved by putting an excess electrostatic charge on the marginally charged hydrogen atoms of the isopropyl moiety. Second, the properties of interest were computed and compared to the experimental densities, viscosities, and diffusion coefficients. Third, the charges were scaled down accordingly since the initially computed charges appeared to suppress molecular dynamics and underestimate the simulated self-diffusion coefficients. Fourth, the sigma parameters of methyl and isopropyl hydrogen atoms were decreased slightly, from 250 pm to 247 pm, to increase the density of the system. Since the sigma parameters of the hydrogen atoms are largely uncertain due to the uniqueness of hydrogen and its chemical inertness in hydrocarbon radicals, the proposed refinement does not introduce unphysical behavior into the MD system. Note that decreasing sigma constants implicitly means increasing the electrostatic attraction energy as some intermolecular distances shrink. This is because the positions of the Lennard-Jones wells determine most equilibrium non-covalent interatomic distances, particularly at lower temperatures. Fifth, the partial charges of the oxygen and hydrogen atoms forming H-bonding were adjusted iteratively to rigorously fit the experimental self-diffusion coefficients and specific densities at 293 K. **Table S3 in the ESI** summarizes the reparameterized partial charges on every atom.

COSMO-RS.

The BIOVIA COSMOtherm 2024 (in short COSMOtherm) program was used to compute thermophysical data on carvacrol-MDSO mixtures, namely their Solid-Liquid Equilibrium (SLE) curve. COSMOtherm is based on COSMO-RS theory.[38,39] COSMO-RS is a statistical thermodynamics approach to predict equilibrium properties in neat and mixed compounds.

The available COSMOtherm release uses input files available in the FINE database for carvacrol and DMSO (using BP-TZVPD_FINE_24 parametrization). The input files contained also the σ-surfaces and σ-profiles of the optimised geometry for DMSO and for the two lowest energy conformers of carvacrol. Melting enthalpy

and temperature for the two compounds[2,19] were extracted from the literature and integrated in the precursor's properties. The Solid-Liquid equilibrium (SLE) option in COSMOtherm was selected and provided the melting temperature for the different mixtures compositions.

Assuming limited change of heat capacity of the compounds, upon melting, the SLE of a component is given by:

$$ln(x_i\gamma_i) = \frac{\Delta H_{m,i}}{R} \cdot \left(\frac{1}{T_{m,i}} - \frac{1}{T}\right) \qquad \textbf{Equation 1}$$

where x_i and γ_i are molar fraction and activity coefficient of the i-th component, respectively, $\Delta H_{m,i}$ and $T_{m,i}$ are the melting enthalpy and temperature of the neat i-th component, respectively, and T is its melting temperature in the mixture at composition x_i. **Equation 1** applies to both components of the mixture, leading to the corresponding melting line of each precursor; their intersection corresponds to the eutectic point.[2] The ideal trend corresponds to the case $\gamma_i = 1$ in **Equation 1**: negative deviations from that trend are associated to non-ideal behaviour and fingerprint the deep nature of the eutectic behaviour.

Results & Discussion

Both carvacrol and DMSO *.cosmo files are included in the COSMOtherm data-base from BIOVIA. They have been evaluated using the BP-TZVPD_FINE_24 parametrization, thus representing the best quality quantum data available from the BIOVIA software at the stage of analysis. These files represent the first stage of quantum chemistry evaluation of the two compounds, paving the way for further analysis by the software. Accordingly, after having included melting parameters (melting enthalpy and temperature, ΔH_m and T_m, respectively) of the precursors (DMSO[2]: ΔH_m =14.37 kJ/mol, T_m = 291.7 K; Carvacrol[19]: ΔH_m =11.49 kJ/mol, T_m = 274.2 K), the Solid-Liquid Equilibrium (SLE) routine has been run, leading to the melting point of the two components as a function of carvacrol molar fraction (Xc). **Figure AAA** reports a comparison between the ideal SLE behaviour (continuous line) and the one evaluated by COSMO-RS (dashed line), accounting for deviation from ideality. Therein, together with the σ-profiles derived from the σ-surfaces (in the insets) from DMSO and the low energy conformers for carvacrol, the COSMO-RS derived SLE line is compared with the ideal behaviour obtained using **Eq. 1**, with unitary activity coefficient. It clearly emerges that COSMO-RS detects a profound deviation from ideal SLE behaviour: while eutectic composition changes only mildly, the eutectic temperature is largely affected by interactions in the mixture and an as large as 110 K decrease in the melting temperature is expected, leading to an eutectic depth $D_e = 100 \cdot \frac{T_e - T_e^{id}}{T_e^{id}} = -44$, one of the lowest values reported so far, to our knowledge.[41] Unfortunately, experimental determination of melting points in these mixtures revealed itself unfeasible, so far. Apart from DMSO-rich mixtures, all the other mixtures show profound supercooling, leading to formation of amorphous glasses that, even after maintaining the liquids for extended time at 180 K, did not lead to formation of crystal phases. Nevertheless, literature reports [3,42] show that COSMO-RS is very efficient in delivering accurate predictions for SLE deviating from ideal behaviour, in agreement with experimental calorimetric data, especially in the case of Type V DES, such as Menthol-Thymol[3,43]. Accordingly, at this stage, we can reliably trust the estimate provided by COSMO-RS for the SLE in carvacrol-DMSO mixtures and derive the conclusion that this system behaves as a deep eutectic one. Such a conclusion can be rationalised in terms of the σ-profiles reported in the inset of **Figure AAA** and shown in the **Figure S2 in ESI**. It clearly emerges that both components are

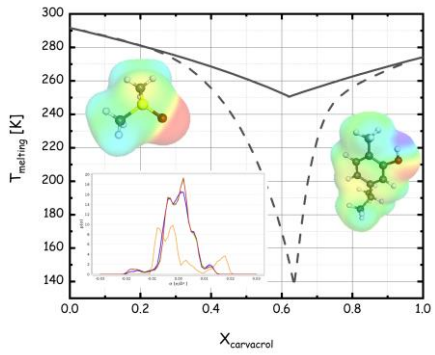

Figure AAA. Solid–liquid equilibrium curves of mixtures composed of carvacrol and DMSO: continuous line, Ideal behaviour; dashed line, COSMOtherm modelling. In the insets, σ-surfaces for DMSO (left) and carvacrol (right) are shown, together with the corresponding σ-profiles.

characterised by a large and intense peak centred at σ~0 e/Å^2; also, in the case of carvacrol, a distinct feature can be detected at σ=-0.016 e/Å^2. Such a feature has no counterpart in the case of DMSO. On the other hand, both carvacrol and DMSO show distinct peaks centred at σ=0.012 and 0.018 e/Å^2, respectively. The large, intense peak near σ ~ 0 e/Å^2 reflects the presence of the electrostatically neutral (apolar) surface regions - aromatic/alkyl surfaces - for carvacrol and methyl-rich surface for DMSO. The distinct negative-σ feature in carvacrol arises from its phenolic acidic proton with a pronounced HB donor behaviour. DMSO has no HBD site, so it quite properly lacks any corresponding negative-σ feature. On the other hand, both molecules exhibit positive-σ peaks that mark HB acceptor character, but at different positions: carvacrol has a modest acceptor peak near σ ≈ +0.012 e/Å^2, associated with the phenolic oxygen lone pairs, whereas DMSO shows a stronger acceptor peak near σ ≈ +0.018 e/Å^2 characteristic of the sulfoxide oxygen. Such a differentiation between the two molecules reflects the driving effect of the asymmetry[4] proposed by Abranches and Coutinho towards the establishment of type V deep eutectic mixtures. The absence of a significant DMSO peak on the negative side of the σ-profile, combined with the clear offset of the positive peaks - DMSO's at higher σ than carvacrol's - leads COSMO-RS SLE predictions to show strong non-ideality in the SLE, consistent with a pronouncedly deep eutectic behaviour. Accordingly, these results strongly support the proposal that selecting precursors by σ-profile comparison represents a practical, predictive route to engineer mixtures that exhibit deep eutecticity.

We next explore several experimental chemical physical properties of carvacrol – DMSO mixtures. Across the discussion, we will also compare experimental findings with Molecular Dynamics (MD) derived corresponding observables, aiming at providing microscopic rationalisation for the macroscopic behaviour.

The temperature and composition dependence of density for binary mixtures across the whole composition range and between 298 and 333 K is shown in **Figure S3** in the ESI. Data (**Table S4 in the ESI**) have been described in terms of linear trend ($\rho(T) = \rho_0 + A \cdot T[K]$) for the temperature dependence with the fitting parameters reported in the **Table S5 in the ESI**. A clear linear dependence is observed as a function of temperature for all the compositions. **Figure CCC** shows the composition dependence of density at 300 K, where MD-derived densities (at the same temperature) are also shown for comparison. A reasonably good agreement is found between experimental and MD-derived density values at 300 K. In **Figure CCC**, 1% error bars are shown for the MD-derived data, reflecting (a lower than) the typical level of agreement

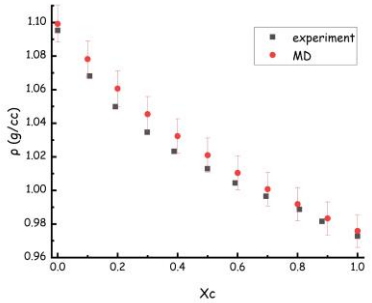

Figure CCC. Comparison between experimental and MD-derived density of carvacrol-DMSO mixtures at 300 K, as a function of Xc.

between experimental density and the one derived from OPLS force fields in MD simulations. Under this condition, the agreement is excellent. Notably the new version of carvacrol FF developed for the present study improves the agreement with experimental density.[23]

The composition and temperature dependence of viscosity in carvacrol-DMSO mixtures are shown in **Figure S4 in the ESI**, together with a description in terms of the VFT formalism. The experimental values and the corresponding fitting parameters are reported in **Table S6 and S7** in the ESI, respectively. As expected, a progressive dropping of viscosity is observed upon increasing temperature. In **Figure EEE**, the viscosity composition dependence is shown at 300 K: it is noteworthy the maximum observed at ca. Xc=0.8, where viscosity is higher than both neat DMSO and carvacrol ones. This behaviour is hinting at the progressive development of strong interactions between the different components that lead to remarkable rigidity of the corresponding mixtures.

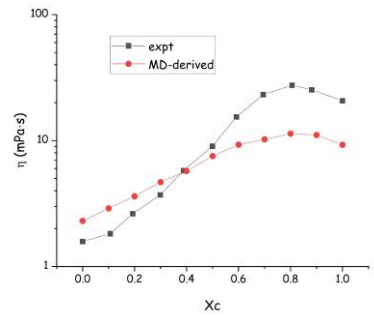

Figure EEE. Viscosity composition dependence for carvacrol-DMSO mixtures at 300 K (black symbols). Data derived from MD simulations are also shown (red symbols).

Experimental density and viscosity values have been used to extract deviation of molar volume, V_m, and viscosity from the ideal behaviour, the corresponding excess quantities, ΔV_m and $\Delta\eta$. ΔV_m and $\Delta\eta$ at 300 K are shown in **Figure XXX**, while their temperature dependence is shown in **Figure S5** of the ESI. These quantities serve as sensitive indicators of deviations from ideality: negative excess volumes or positive excess viscosities typically signal the establishment of preferential interactions and structural compaction, whereas opposite trends usually reflect geometric or excluded-volume effects, pointing to disrupted molecular packing and/or weaker intermolecular cohesion.

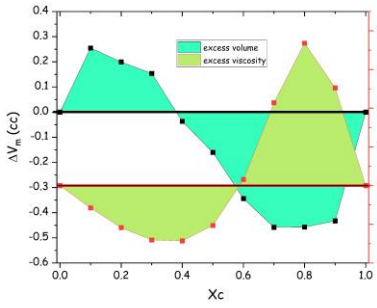

Figure XXX. Excess molar volume (ΔV_m, black curve, left axis), and viscosity ($\Delta\eta$, red curve, right axis) at 300 K for carvacrol-DMSO mixtures.

In **Figure XXX**, we note the highly structured evolution of these quantities. In particular, we highlight a complementary behaviour: across the equimolar range, excess extremes are found with opposite sign for excess molar volume and viscosity. At low carvacrol content, positive excess volume and negative excess viscosity are found; while the opposite behaviour is found in the carvacrol-rich composition regime. This observation is consistent with a DMSO-rich regime, where progressive carvacrol addition leads to an expansion of the mixture, hence the ΔV_m maximum at Xc~0.1, and a corresponding decreasing of excess viscosity, hence the minimum of $\Delta\eta$ at Xc~0.35. At higher carvacrol content, the opposite behaviour occurs with a pronounce volume contraction,

corresponding to a strong increase of viscosity at Xc~0.8. This crossover reflects a competition between geometric packing effects at low donor fractions and strong donor–acceptor interactions at higher carvacrol fractions. When Xc is small, geometric packing dominates, leading to volume expansion and keeping viscosity low; on the other hand, as DMSO is added to neat carvacrol, the emergent donor–acceptor (O–H···O=S) network compacts the liquid and dynamically frustrates motion, driving a pronounced viscosity rise. In short, packing governs the carvacrol dilute regime, while specific hetero-interactions take over at higher carvacrol fractions, coherently shaping both properties. Likely, this behavior is driven by the emergence of a topologically connected O–H···O=S hydrogen-bond network that marks the crossover: as connectivity approaches saturation, cooperative constraints compact the liquid and hinder molecular mobility. Crucially, this network emerges at a threshold composition, signaling a composition-driven transition.

The establishment of progressively topologically saturated HB network, upon increasing DMSO content, looks like a fundamental stage to ensure complete donor-acceptor engaging leading to maximum enthalpic gain and structural correlations between the precursors, with volume compaction and increased local rigidity. We will ascertain further support to this picture on the basis of other experimental and computed results, across the manuscript: at the present stage, we note that the eutectic location corresponds to a balance between the inefficient packing of differently shaped and sized molecules (low carvacrol content regime) and a progressively saturating HB network between unlike HBD and HBA (carvacrol rich regime).

We next determined the ^{1}H NMR diffusion coefficients (DC) for both species in the mixtures at 300 K. Data are shown in **Figure FFF**, together with the corresponding parameters obtained from MD simulations (open symbols). We used logarithmic scale for plotting these data: this approach enhances differences between data values that are quite close instead. Upon addition of carvacrol to neat DMSO, both DMSO and carvacrol DCs decrease, reflecting the increasing viscosity environment. Carvacrol maintains twice slower than DSMO. When approaching Xc=0.5, however, DMSO DC increases its dropping rate and, eventually, at ca. Xc=0.7, DMSO turns out to diffuse slower than carvacrol. Further increase in carvacrol content leads to the development of a faint minimum feature, with the difference between DMSO and carvacrol DC further increasing, DMSO diffusing slower than carvacrol. Mirroring the observations done on excess properties, these trends reflect the occurrence of a structural-dynamic transition, across composition Xc=0.5-0.6. Below this threshold, a strong evolution of DC is observed with a decrease of a factor of 5 from Xc equal 0 to 0.5-0.6. Above the threshold, an almost constant

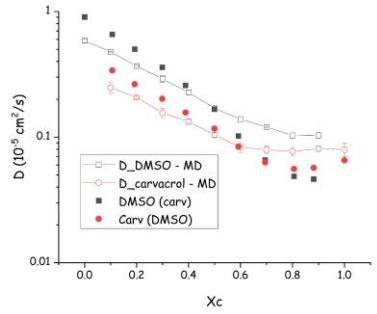

Figure FFF. ^{1}H NMR diffusion coefficients (DC) for carvacrol and DMSO in their mixtures at 300 K (filled symbols). Open symbols refer to corresponding quantities obtained by MD simulations.

behaviour is found instead. The dynamic scenario emerging from these data can be rationalised in terms of the above mentioned packing vs topological HB saturation competition. Upon adding DMSO to carvacrol, progressive formation of donor-acceptor combination occurs. In this regime, until completion (at ca. equimolar conditions), the diffusion behaviour experimentally shows a mild decrease in diffusion dyanmics, consistently with the enhanced excess viscosity. Upon saturation of carvacrol HBD capability, dynamic HB paired DMSO-carvacrol entities characterise the structural scenario and, with further DMSO addition, above equimolar regime, these strongly bound pairs are only diluted, leading to a progressive increase in diffusive dynamics.

Overall, there is an excellent agreement between experimental and computed diffusion coefficients (evaluated with the new FF for carvacrol), although we detect minor qualitative differences in the trend of MD–derived data that do not follow accurately the experimental trend.

The experimental data have been interpreted together with viscosity data, in terms of the Stokes Einstein relationship (under stick boundary conditions):

$$D_i = \frac{k_B T}{6\pi \cdot \eta \cdot R_{h,i}}$$

(D_i is the diffusion coefficient of i-th species, k_B is the Boltzmann constant, T is the absolute temperature, η is the mixture viscosity and $R_{h,i}$ is the hydrodynamic radius of the i-th species), extracting estimates for the hydrodynamic radius of either DMSO ($R_{h,DMSO}$) or carvacrol ($R_{h,carv}$). Fitting experimental data to this model delivers values for $R_{h,DMSO}$ and $R_{h,carv}$ equal to 1.62 and 3.0 Å, respectively. When using these experimentally derived $R_{h,i}$'s together with MD-derived diffusion coefficients for the two species, we can extract the corresponding estimations for viscosity of the mixtures, by reversing the use of the Stokes-Einstein relationship. The average of the two so obtained viscosities is shown in **Figure EEE** comparing with the experimental viscosity. The agreement between such a hybrid determination of MD-derived viscosity (based on the improved FF for carvacrol) and experimental values is remarkable: despite quantitative agreement is not achieved, nevertheless, the qualitative experimental observation of a viscosity maximum at ca. Xc=0.8 is accurately reproduced.

We next explored the nature of structural properties as detected by X-ray/neutron scattering. The improved FF for carvacrol did not lead to appreciable differences in the already remarkable agreement between

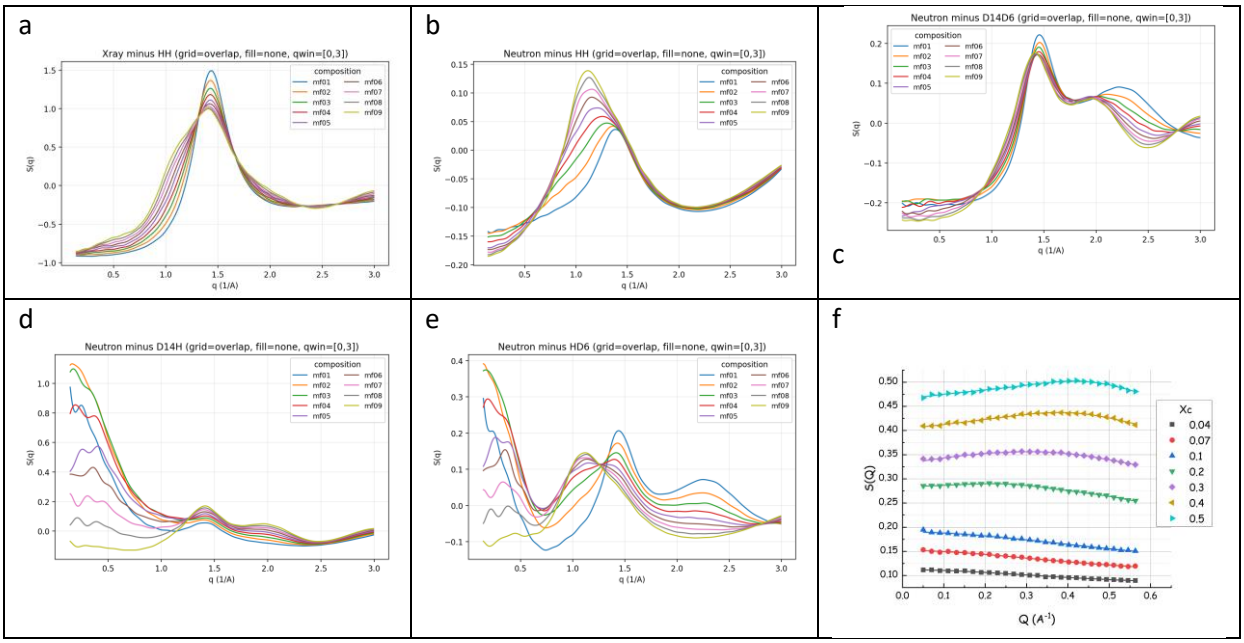

Figure GGG. MD derived X-ray (a) and neutron (b-e) weighted structure factors for carvacrol-DMSO mixtures as a function of composition at 300K. Neutron weighted structure factors refer to different level of selective deuteration: namely: b) both components protiated; c) both components deuterated; d) only carvacrol deuterated; e) only DMSO deuterated. Also shown in f) experimental SANS data from only DMSO deuterated mixtures at selected composition. Therein, lines correspond to the fit described in the text. Vertical shift is not artificial, but due to the incoherent protium scattering from carvacrol.

experimental and MD-derived X-ray weighted static structure factor for neat carvacrol.[23] In **Figures GGG**, the X-ray (a) and neutron (b-e) weighted static structure factors (in the case of neutron scattering, no deuteration, selective deuteration of either carvacrol or DMSO or both components have been considered) are shown over the Q range up to 3.0 $Å^{-1}$, which is the relevant Q range to probe intermolecular correlations. In **Figure GGG f)**, we also report experimental Small Angle Neutron Scattering (SANS) data for the selectively deuterated mixture HD6 (mixtures of protiated carvacrol with fully deuterated DMSO) together with their fit with the model described in the following. A direct comparison with **Figure GGG e)** cannot be done, as normalizations of the experimental and computed S(Q)s are different.

X-ray scattering curves deliver a structural scenario consistent with the nano-structured carvacrol organization, which is progressively influenced by DMSO addition, leading to a systematic shift of the low Q peak centred at ca. 0.5 $Å^{-1}$, towards lower Q values. This trend seems to be consistent with the progressive distancing of those nano-clusters of interacting hydroxyl group, due to DMSO intrusion. Neutron scattering data related to mixtures with small contrast arising from selective deuteration (i.e. those mixtures with no or both components deuterated) provide a similar picture. Due to Babinet's principle[3], the two selectively deuterated (either at carvacrol or at DMSO) systems, deliver neutron scattering data that, in the low Q range, are quite

similar. Therein, however, a higher degree of complexity emerges concerning the mesoscopic organization, with respect to X-ray weighted data. These hints are also confirmed by the experimental SANS patterns that were collected in the DMSO-rich range of the composition.

Experimentally, below Xc=0.1, indications of concentration fluctuations at the mesoscopic scale are found, fingerprinted by the distinct upturn at low Q. Data have been modelled using the Ornstein−Zernike formalism:

$$I(Q) = \frac{I_0}{1+\xi^2 \cdot Q^2} - bkg;$$

where I_0 is the coherent forward scattering intensity, ξ is the correlation length, measuring the spatial decay of concentration correlations, and bkg is a flat background term that is mainly arising from the incoherent scattering from the protium atoms in carvacrol. In the composition range between Xc=0 and 0.2, I_0 increases and ξ decreases with DMSO content. Above Xc=0.1, the concentration fluctuations feature is progressively overcome by the appearance of two peaks, whose position evolves with composition. In that composition range, the SANS signal is dominated by two peaks (modelled with Gaussian shape) at positions, Q_i (i=1, 2), shifting to lower Q values, upon increasing DMSO content. The resulting fit is shown in **Figure GGG e)**, while we show in **Figure S5** in the ESI, the Xc dependence of ξ and $D_i=2\pi/Q_i$, where D_i are the spatial scales associated to the i-th peaks. All these sizes grow with increasing DMSO content. The characteristic size of concentration fluctuation, ξ, grows in the range of a few Å, fingerprinting the approach to microphase separation in DMSO rich mixtures. D_2, the spatial scale corresponding to the higher Q value, falls in a range consistent with the previously reported clusters characterising the structure of phenolic compounds, including phenol and terpenes (such as thymol), where a low Q peak is observed in the X-ray scattering pattern at ca. 0.5 $Å^{-1}$. This feature is associated to the hydrogen bonding mediated aggregation of hydroxyl group, forming nano-drops, surrounded by aromatic/alkyl apolar moieties. Such a structural organization is characterised by a spatial scale of the order of 1 nm. In carvacrol-DMSO mixtures, progressive DMSO addition leads to a growth of this size, due to DMSO intruding inside both the polar and apolar portion, due to DMSO amphiphilicity. The spatial scale associated to the lower Q value peak, D_1, also grows with increasing DMSO content, raising from 27 Å (at Xc=0.5) up to 47 Å (at Xc=0.2, the lowest value where it could be detected). Such a feature has no counterpart neither in neat DMSO nor in neat carvacrol. Considering its notable growth, it could potentially considered a sort of precursor of the concentration fluctuations that become appreciable at Xc=0.2, but at the present stage, we cannot formulate a more robust explanation of its nature.

Aiming at getting deeper insight into the structural features characterising carvacrol-DMSO, we further inspected the MD trajectories. The first observable that can provide some indication of structural evolution is the spatial correlation between neighbour molecules. We determined the center-of-mass (CoM) pair distribution functions (pdf) between like and distinct species (**Figure ZZZ**). DMSO-DMSO pdfs look largely

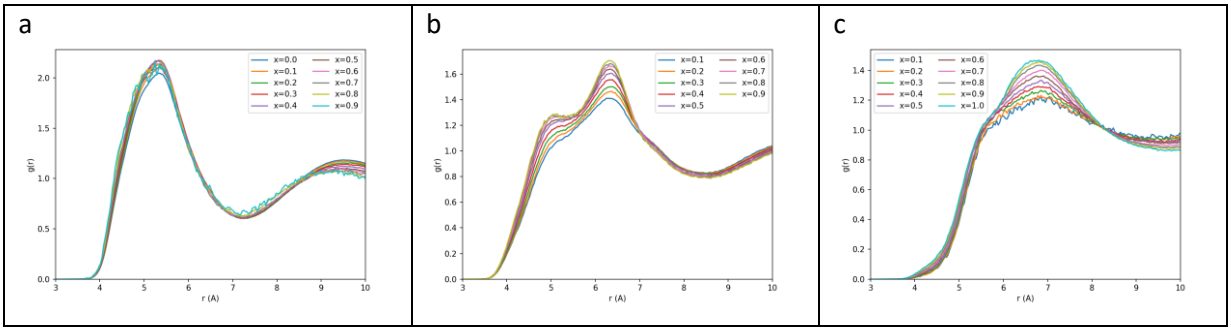

Figure ZZZ. Center of Mass pair distribution functions between a) DMSO-DMSO, b) carvacrol-DMSO and c) carvacrol-carvacrol pairs in MD simulations of carvacrol-DMSO mixtures at 300 K.

unaffected by addition of carvacrol: a rather structured peak is found at ca. 5.5 Å, related to dipole-dipole alignment of DMSO molecules in the fluid. The interspecies pdfs (carvacrol-DMSO) are characterised by a structured peak with features at 5, 6.5 and 7.5 Å. Only the latter one is unaffected by composition. In the case of carvacrol-carvacrol pdfs, the first solvation shell, extends up to 10 Å, but it is characterised by a relatively unaffected shoulder centred at ca. 5.5 Å. In order to better describe these correlations, we monitored the number of first neighbours up to the mentioned first shell of solvation (i.e. up to 7, 5.5 and 6 Å, for DMSO-DMSO, DMSO-carvacrol and carvacrol-carvacrol, respectively). These neighbour numbers are plotted in the **Figure S6** in ESI and they show interesting features.

Upon carvacrol content increase: a) DMSO-DMSO correlations show a progressively decreasing number of neighbours (notice that in **Figure S6** these data are vertically shifted by 3) evolving from ca. 12 (in neat DMSO) down to ca. 0.7 (for Xc=0.9); b) the number of DMSO molecules surrounding a reference carvacrol progressively decreases from 2.5 to 0.2; c) the number of carvacrol molecules surrounding a reference carvacrol progressively increases from 0.3 up to 1.8. It is noteworthy that these trends can be considered as built up by different linear trends across a composition threshold. We highlighted such a feature, by plotting the mentioned linear trends accounting for number of neighbours before and after the composition threshold and it is visually clear that the regime transition occurs across equimolar composition. This observation provides further support to the existence of a structural transition across a composition threshold.

We next examined hydrogen-bond correlations in the mixtures. Carvacrol can act as both a hydrogen-bond donor and acceptor, whereas DMSO acts only as a strong hydrogen-bond acceptor. The interaction between these two components is therefore governed primarily by hydrogen bonding, which drives the structural organization of the mixtures as the composition changes. **Figures S7** in the ESI show the relevant Hc-Oc and Hc-Od pdfs, referring to the carvacrol hydroxyl species Hc and Oc and the DMSO oxygen one, Od. The corresponding number of neighbour oxygen atoms (either from carvacrol (N [Hc-Oc]=Ncc) or from DMSO (N [Hc-Od]=Ncd) or both (N [Hc-Oc] + N [Hc-Od]) = Nt) surrounding carvacrol Hc atom via an HB interaction is reported in **Figure III**. Both pdfs are characterised by a strong peak at ca. 2 Å, a distinct signature of the existence of a HB interaction between the probed species; however, Hc-Od are characterised by a much stronger peak than Hc-Oc, reflecting more intense DMSO HB acceptor nature. Upon increasing carvacrol content, the number of Oc coordinating Hc progressively increases. Concomitantly, the number of Od coordinating Hc progressively decreases. The limited HB acceptor ability of carvacrol can be appreciated by the small number of HB interactions in neat carvacrol, so that the total number of HB interaction per Hc species decreases from 1 (Xc=0.1) to 0.5 (Xc=1).

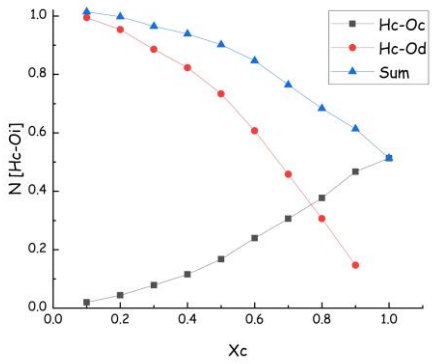

Figure III. MD derived number of neighbour oxygen atoms (either from carvacrol (N [Hc-Oc]=Ncc) or from DMSO (N [Hc-Od]=Ncd) or both (N [Hc-Oc] + N [Hc-Od]) = Nt) surrounding carvacrol Hc atom via an HB interaction, as a function of carvacrol content.

The MD-derived population of HB interactions was used to rationalise the experimental ^{1}H NMR chemical shift determined for the hydroxyl proton in carvacrol. While all other protons in the mixtures showed a monotonous and featureless trend with composition (data not shown), the former proton showed a non-linear behaviour as reported in **Figure LLL**. The fluctuations in the hydrogen bond network involving these hydrogen atoms occur on a very short timescales (picoseconds), enabling a single averaged NMR peak to emerge. The corresponding observed chemical shift is thus a population-weighted average of the different limiting chemical environments: we used the above discussed MD-derived coordination numbers - interpreted as the fraction of OH groups engaged in hydrogen bonds (with either carvacrol or DMSO) or not – to try and reproduce the NMR trend.

We found an excellent agreement between the experimental ^{1}H-NMR chemical shift of the hydroxyl proton, H_c, ($\delta_{Hc,exp}$), in carvacrol–DMSO mixtures and the hydrogen bonding population derived from MD simulations in terms of a three-state fast exchange model. In this framework, carvacrol H_c, rapidly fluctuates among three local environments, each corresponding to a specific chemical shift: (1) hydrogen-bonded to DMSO (δ_{DMSO}), (2) hydrogen-bonded to another carvacrol molecule (δ_{self}), and (3) non-hydrogen-bonded or weakly solvated (e.g. via $H_c \cdots \pi$ HB interactions) (δ_{free}). Using: a)the chemical shift experimentally determined for neat carvacrol (6.63 ppm) for δ_{self}, b) the linearly extrapolated value of the observed chemical shift for Xc⟶0 for δ_{DMSO} and c) considering δ_{free} as the only fitting parameter to reproduce the experimental data, we modelled the experimental data in terms of the following relationship:

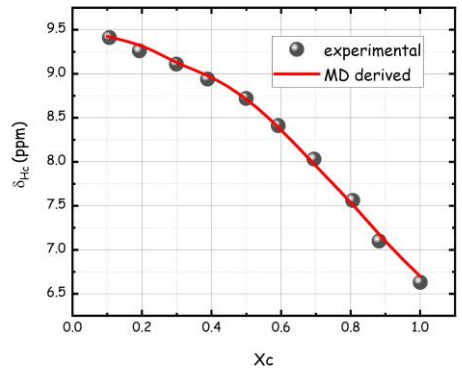

Figure LLL. Experimental ^{1}H NMR chemical shift for Hc in carvacrol (symbols) and its modelling (line) in terms of the hydrogen bonding pairs populations obtained by MD simulations (see the text for details).

$$\delta_{H_c,exp} = N_{cc}\delta_{self} + N_{cd}\delta_{DMSO} + (1 - N_t)\delta_{free},$$

where Ncc+Ncd+Nt=1. By modelling the experimental chemical shift data, $\delta_{Hc,exp}$, with this three-state model, one obtains that δ_{free} is slightly more deshielded than δ_{self} — a non-intuitive but chemically plausible outcome, considering the heterogeneous environment where carvacrol hydroxyl group is immersed. The overall consistency of the model with experimental data provides strong validation for both the force field used in the simulations and the assumption of fast exchange on the NMR timescale, providing a unified molecular-level explanation of the spectroscopic behavior.

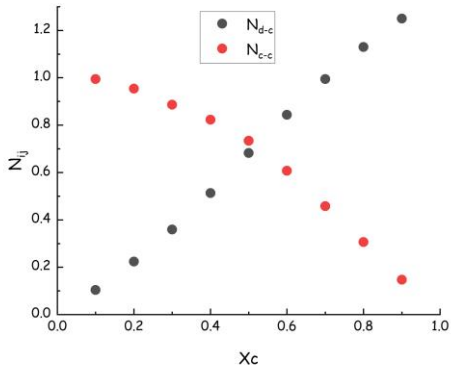

Figure QQQ. Number of Hc atoms HBd to DMSO O atoms, Ndc, compared to number of Od atoms HBd to carvacrol Hc atoms, Ncd, as a function of carvacrol content.

We also monitored the number of Hc atoms surrounding DMSO O atoms, as a function of carvacrol content, N [Od- Hc]=Ndc. This number is shown in **Figure QQQ**, together with Ncd, from the previous analysis. Ndc can assume values higher than one at carvacrol rich compositions, due to the possibility to establish HB interactions with more than one Hc carvacrol atoms. The comparison reported in **Figure QQQ** is noteworthy: in order to maximise enthalpy-

rewarding hydrogen bonding interactions between hetero-species, the best composition corresponds to the condition when both Ndc and Ncd are maximised. Inspection of **Figure QQQ** suggests that such an optimal composition is slightly above Xc=0.5. Considering the asymmetry in HB capabilities of the two components, this results might have been expected and is a consequence of the knowledge-driven selection of DMSO as a lone HBA precursor combined with the asymmetric HBD carvacrol, to engineer the formulation of type V DES.

We finally explored dynamic features associated to hydrogen bonding interactions in the mixtures. **Figures MMM** reports MD-derived intermittent lifetime relaxation behaviour for carvacrol-carvacrol (a), $I_{HB\text{-}CC}(t)$) and carvacrol-DMSO (b) $I_{HB\text{-}CD}(t)$) hydrogen bonding interactions as well as relaxation dynamics of DMSO S-O vector (c) $I_{SO}(t)$). These data have been modelled with a bimodal dynamics, build up by the combination of a simple exponential and stretched exponential components:

$$I(t) = A \cdot e^{-\frac{t}{\tau_f}} + (1 - A) \cdot e^{-\left(\frac{t}{\tau_{KWW}}\right)^{\beta}},$$

where A is the amplitude of a fast, prevalently out of the probed temporal window (faster than picosecond), process, τ_f is its characteristic temporal scale, τ_{KWW} is the time scale of the slow, stretched exponential relaxation process and β is the stretching exponent.

The three characteristic times, $<\tau_{KWW}>$, for the processes have been determined:

$$< \tau_{KWW} >= \tau_{KWW} \cdot \Gamma\left(\frac{1}{\beta}\right);$$

where Γ(..) is the Gamma function; and are plotted in **Figure MMM d)**. The bimodal dynamics accounts for

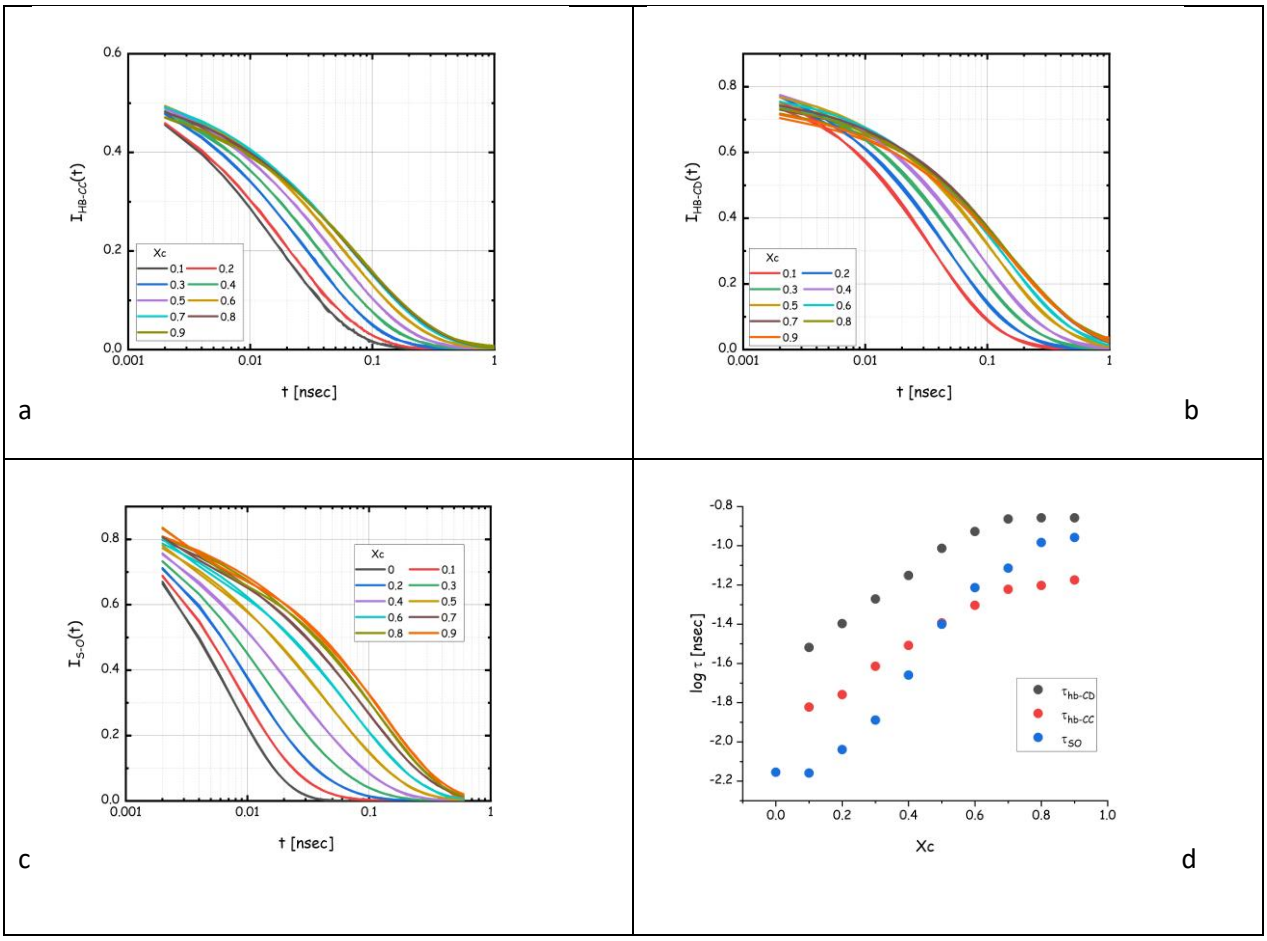

Figure MMM. Composition dependence of the MD-derived hydrogen bonding relaxation dynamics for a) carvacrol-carvacrol and b) carvacrol-DMSO hydrogen bonding interactions. c) Composition dependence of the MD derived relaxation dynamics of DMSO S-O vector. d) Composition dependence of the slow characteristic times of the three relaxation processes.

the whole relaxation process over three decades. The three slow relaxations probed are characterised by a temporal scale of the order of 0.1 nsec. The hydrogen bonding lifetime associated to carvacrol-DMSO pairs has longer life than the one associated to carvacrol-carvacrol pairs by a factor of ca. 2. The two average relaxation times follow a parallel behaviour as a function of composition, with a visible break at ca. Xc=0.6. Also the S-O vector relaxes with a time scale of the order of 0.1 nsec: it is quite slow at high carvacrol content (reflecting the strong engagement of S=O with carvacrol hydroxyl group), but gets very fast as approaching neat DMSO. We notice that this relaxation shows a larger composition dependence in terms of relaxation time. Again, a characteristic break in composition dependence is observed at Xc= 0.5-0.6. These dynamic characterizations provide further support to the existence of crossover across Xc= 0.5-0.6, reflecting the transition between two regimes: one (carvacrol-rich) where inter-species correlations via HB interactions is strong and rigid and another (DMSO-rich) where excess DMSO merely dilutes already HB engaged pairs.

Conclusion.

Acknowledgements.

This work has been supported by the University of Rome Sapienza Projects: "Chemical physical properties and solvation capability of water-based eutectic solvents." (RM123188F106B148). Research at ISM-CNR was supported by the project ECS00000024 “Ecosistemi dell’Innovazione”— Rome Technopole of the Italian Ministry of University and Research, public call n. 3277, PNRR— Mission 4, Component 2, Investment 1.5, financed by the European Union, Next GenerationEU. This work was also supported by PRIN2022 (“SEED4GREEN”), sponsored by the European Union, Next Generation EU, Missione 4 Componente 1 (RG11715C7CC660BE).

Access to the Budapest Reactor…..

References.

1 A. P. Abbott, G. Capper, D. L. Davies, R. K. Rasheed and V. Tambyrajah, *Chem. Commun. (Camb).*, 2003, 70–71.

2 E. L. Smith, A. P. Abbott and K. S. Ryder, *Chem. Rev.*, 2014, **114**, 11060–11082.

3 D. O. Abranches, M. A. R. Martins, L. P. Silva, N. Schaeffer, S. P. Pinho and J. A. P. Coutinho, *Chem. Commun.*, 2019, **55**, 10253–10256.

4 D. O. Abranches and J. A. P. Coutinho, *Curr. Opin. Green Sustain. Chem.*, 2022, **35**, 100612.

5 N. Schaeffer, D. O. Abranches, L. P. Silva, M. A. R. Martins, P. J. Carvalho, O. Russina, A. Triolo, L. Paccou, Y. Guinet, A. Hedoux and J. A. P. Coutinho, *ACS Sustain. Chem. Eng.*, 2021, **9**, 2203–2211.

6 C. R. Ashworth, R. P. Matthews, T. Welton and P. A. Hunt, *Phys. Chem. Chem. Phys.*, 2016, **18**, 18145–18160.

7 C. F. Araujo, J. A. P. Coutinho, M. M. Nolasco, S. F. Parker, P. J. A. Ribeiro-Claro, S. Rudić, B. I. G. Soares and P. D. Vaz, *Phys. Chem. Chem. Phys.*, 2017, **19**, 17998–18009.

8 O. S. Hammond, D. T. Bowron and K. J. Edler, *Green Chem.*, 2016, **18**, 2736–2744.

9 M. A. R. Martins, E. A. Crespo, P. V. A. Pontes, L. P. Silva, M. Bülow, G. J. Maximo, E. A. C. Batista, C. Held, S. P. Pinho and J. A. P. Coutinho, *ACS Sustain. Chem. Eng.*, 2018, **6**, 8836–8846.

10 D. O. Abranches and J. A. P. Coutinho, *Annu. Rev. Chem. Biomol. Eng.*, 2023, **14**, 141–163.

11 Q. Liu, H. Mou, W. Chen, X. Zhao, H. Yu, Z. Xue and T. Mu, *Ind. Eng. Chem. Res.*, 2019, **58**, 23438–23444.

12 E. L. Byrne, R. O'Donnell, M. Gilmore, N. Artioli, J. D. Holbrey and M. Swadźba-Kwaśny, *Phys. Chem. Chem. Phys.*, 2020, **22**, 24744–24763.

13 T. El Achkar, T. Moufawad, S. Ruellan, D. Landy, H. Greige-Gerges and S. Fourmentin, *Chem. Commun.*, 2020, **56**, 3385–3388.

14 T. El Achkar, L. Moura, T. Moufawad, S. Ruellan, S. Panda, S. Longuemart, F.-X. Legrand, M. Costa Gomes, D. Landy, H. Greige-Gerges and S. Fourmentin, *Int. J. Pharm.*, 2020, **584**, 119443.

15 A. Triolo, F. Lo Celso, S. Fourmentin and O. Russina, *ACS Sustain. Chem. Eng.*, 2023, **11**, 9103–9110.

16 E. Mangiacapre, A. Triolo, M. Kfoury, S. Ruellan, F. Lo Celso, D. J. M. Irving, S. Fourmentin and O. Russina, *Carbohydr. Polym.*, 2025, **366**, 123819.

17 W. Mączka, M. Twardawska, M. Grabarczyk and K. Wińska, *Antibiotics*, 2023, **12**, 824.

18 V. Gandova, A. Lazarov, H. Fidan, M. Dimov, S. Stankov, P. Denev, S. Ercisli, A. Stoyanova, H. Gulen, A. Assouguem, A. Farah, R. Ullah, M. Kara and A. Bari, *Open Chem.*, 2023, **21**, 20220319.

19 A. Alhadid, L. Mokrushina and M. Minceva, *J. Mol. Liq.*, 2020, **314**, 113667.

20 B. Hess, C. Kutzner, D. van der Spoel and E. Lindahl, *J. Chem. Theory Comput.*, 2008, **4**, 435–447.

21 D. Van Der Spoel, E. Lindahl, B. Hess, G. Groenhof, A. E. Mark and H. J. C. Berendsen, *J. Comput. Chem.*, 2005, **26**, 1701–1718.

22 C. Caleman, P. J. van Maaren, M. Hong, J. S. Hub, L. T. Costa and D. van der Spoel, *J. Chem. Theory Comput.*, 2012, **8**, 61–74.

23 E. Mangiacapre, A. Triolo, F. Ramondo, F. Lo Celso and O. Russina, *J. Mol. Liq.*, 2024, **394**, 123778.

24 E. Mangiacapre, F. Lo Celso, A. Triolo, F. Ramondo, D. J. M. Irving, A. Alhadid, M. Minceva, O. Russina and J. Daniel, *J. Phys. Chem. B*, 2025, **129**, 3224–3236.

25 W. L. Jorgensen and J. Tirado-Rives, *Proc. Natl. Acad. Sci.*, 2005, **102**, 6665–6670.

26 L. Martínez, R. Andrade, E. G. Birgin and J. M. Martínez, *J. Comput. Chem.*, 2009, **30**, 2157–2164.

27 G. Bussi, D. Donadio and M. Parrinello, *J. Chem. Phys.*, 2007, **126**, 014101.

28 M. Parrinello and A. Rahman, *J. Appl. Phys.*, 1981, **52**, 7182–7190.

29 T. Darden, D. York and L. Pedersen, *J. Chem. Phys.*, 1993, **98**, 10089–10092.

30 U. Essmann, L. Perera, M. L. Berkowitz, T. Darden, H. Lee and L. G. Pedersen, *J. Chem. Phys.*, 1995, **103**, 8577–8593.

31 M. Brehm and B. Kirchner, *J. Chem. Inf. Model.*, 2011, **51**, 2007–2023.

32 O. Hollóczki, M. Macchiagodena, H. Weber, M. Thomas, M. Brehm, A. Stark, O. Russina, A. Triolo and B. Kirchner, *ChemPhysChem*, 2015, **16**, 3325–3333.

33 M. Brehm, M. Thomas, S. Gehrke and B. Kirchner, *J. Chem. Phys.*, 2020, **152**, 164105.

34 R. Peverati and D. G. Truhlar, *Phys. Chem. Chem. Phys.*, 2012, **14**, 11363–11370.

35 F. Weigend and R. Ahlrichs, *Phys. Chem. Chem. Phys.*, 2005, **7**, 3297–3305.

36 U. C. Singh and P. A. Kollman, *J. Comput. Chem.*, 1984, **5**, 129–145.

37 M. W. Schmidt, K. K. Baldridge, J. A. Boatz, S. T. Elbert, M. S. Gordon, J. H. Jensen, S. Koseki, N. Matsunaga, K. A. Nguyen, S. Su, T. L. Windus, M. Dupuis and J. A. Montgomery, *J. Comput. Chem.*, 1993, **14**, 1347–1363.

38 F. Eckert and A. Klamt, *AIChE J.*, 2002, **48**, 369–385.

39 A. Klamt and F. Eckert, *Fluid Phase Equilib.*, 2000, **172**, 43–72.

40 E. S. Domalski and E. D. Hearing, *J. Phys. Chem. Ref. Data*, 1996, **25**, 1.

41 A. van den Bruinhorst and M. Costa Gomes, *Curr. Opin. Green Sustain. Chem.*, 2022, **37**, 100659.

42 B. Bernicot, G. Arrachart, S. Dourdain, N. Schaeffer, G. Teixeira and S. Pellet-Rostaing, *J. Mol. Liq.*, 2025, **427**, 127332.

43 G. Teixeira, D. O. Abranches, L. P. Silva, S. M. Vilas-Boas, S. P. Pinho, A. I. M. C. L. Ferreira, L. M. N. B. F. Santos, O. Ferreira and J. A. P. Coutinho, *Molecules*, 2022, **27**, 2649.

44 L. A. Feigin and D. I. Svergun, *Structure Analysis by Small-Angle X-ray and Neutron Scattering*, New York, NY USA, 1987.